Investigating Turbulent Dynamics in the Nocturnal Boundary Layer: A Large Eddy Simulation Study of the South Fork Wind Farm

Adam Ayouche[1], Baylor Fox-Kemper[1], Yongjie Liu[2] and Georgios Matheou[2]

[1]Department of Earth, Environmental, and Planetary Sciences (DEEPS), Brown University, Providence, RI, USA
[2]Department of Mechanical, Aerospace and Manufacturing Engineering, University of Connecticut, Storrs, CT, USA

E-mail: adam_ayouche@brown.edu

Abstract.

In this study, Large Eddy Simulations (LES) with realistic inflow conditions are conducted to investigate the dynamics of the nocturnal marine atmospheric boundary layer (MABL) (with approximately 8 m/s mean inflow speeds) around the South Fork Wind Farm, completed in March 2024 and located 35 miles offshore and east of Montauk Point, NY. The LES framework incorporates 12 turbines represented by actuator disk models. We analyze the turbulence and circulation dynamics in the wake regions, focusing on the effects of tilting and stretching on vorticity. Our findings reveal that these processes intensify circulation and induce convergent (upward) motions in the near wake, while acting as sinks of vorticity in the far wake, thereby weakening circulation and facilitating flow recovery mechanisms. Additionally, we identify shear production as the primary source of turbulent kinetic energy (TKE) downstream of the actuator discs, peaking above the hub height, particularly at the top tip. The consistently upward buoyancy flux supports the summertime nocturnal boundary layer dynamics, with heating at the surface inducing convective buoyancy also producing TKE, observed in our simulations. Overall, TKE is primarily removed through dissipation and transport.

1 Introduction

Wind power is projected to supply 20% of global electricity demand by 2030 [1]. Turbines extract kinetic energy from the wind, reducing wind speeds [2]. This extraction modifies the wind flow and influences turbulence and stratification in the wake region [3, 4, 5]. Changes in stratification are closely linked to variations in surface temperature gradients and momentum fluxes, particularly in stable atmospheric boundary layers (ABLs) that are typical of nighttime boundary layers over land, where turbulence is suppressed and turbulent mixing is weak [6, 7, 5]. Unstable, or convective, conditions can also produce turbulence through buoyancy production via heating and moistening of the atmosphere from below, typically at the surface. Typically, convective conditions are encountered when the surface is heated by the sun or in a marine atmospheric boundary layer (MABL) through evaporation and upward moisture transport in the atmosphere. Presently, a nighttime MABL is investigated. Unlike nocturnal boundary layers over land, in the present MABL night-time conditions results in a shallow convective layer. The layer is shallower than daytime conditions since at night the surface buoyancy flux is reduced. Installing

wind farms can induce local atmospheric changes, affecting vegetation, air temperature, and the dynamics of the ABL [8, 9, 10]. Notably, when the ABL is somewhat thicker than the height of the turbines, the turbulence generated by the turbines is not confined to the hub height but extends throughout the ABL, further influencing local climatic conditions.

These local changes, resulting from the momentum deficit caused by the turbines and variations in ABL stratification, are primarily confined to the wake region downstream of the turbines. This wake region is critical, as it can lead to significant power losses across wind farms when the wake of one or more turbines affects those further downstream, mainly due to farm layout, wind shear, and ABL stability. The (in)stability of the ABL induces local alterations in wind shear directions and buoyancy forcing, which further complicate the wake dynamics [11, 12, 13]. Moreover, diurnal and seasonal variations of the ABL affect the transport of heat and the surface release/absorption of heat, momentum fluxes, and turbulent energy transport [14]. Numerous studies have focused on wake turbulence and spreading in neutral, stable, and convective conditions, both with and without considering the Coriolis effect (e.g., [15, 16, 17]). These studies highlight the substantial impact of ABL regimes on wind farm wake dynamics. Different ABL regimes can significantly alter the dynamics downstream of wind turbines; however, most wind tunnel experiments and many engineering models have primarily addressed uniform density and neutral boundary layer inflow conditions [18, 19, 20]. As turbine rotor sizes continue to grow, the role of stratified free troposphere dynamics above the ABL are expected to become more pronounced, emphasizing the necessity of understanding wake region dynamics under varying conditions. Indeed, in many regions and seasons, including the South Fork site, turbines seasonally protrude above the ABL [21, 22].

Efforts have been made to capture the dominant wake dynamics using different models. One-dimensional (1D) models, based primarily on momentum theory, predict the momentum deficit in the wake by assuming a self-similar Gaussian profile; however, they often overlook the direct and indirect effects of atmospheric stratification, limiting their accuracy in turbulent conditions [23, 24]. Engineering models, such as those from Crespo and Hernández [25], incorporate empirical turbulence parameters, but tend to neglect the underlying ABL physics, making them less reliable under varying stability conditions. In contrast, Reynolds Averaged Navier–Stokes (RANS) models and dynamic wake meandering (DWM) models provide a more comprehensive approach by solving (a form of) the Navier–Stokes equations, thus capturing more complex wake physics [26, 27, 28, 29]. These models still rely on various turbulence-modeling assumptions, such as averaging over extended periods and simplifying the degrees of freedom, which may fail to capture turbulence anisotropy and variability accurately. This is particularly pronounced in strongly convective and stable atmospheric boundary layers, where the complexities of turbulent flows can significantly influence wake dynamics and recovery [30, 31].

In the present work, Large-Eddy Simulations (LES) are carried out using uniform actuator discs [32] representing the 12 turbines, nominally generating 132 MW, built offshore of Montauk, NY. These 12 turbines are part of the South Fork project (https://southforkwind.com), which was completed in March 2024. Using the layout of the South Fork wind farm allows us to capture the wake dynamics and interactions with a fair-weather nocturnal summertime boundary layer, mainly characterized by prevailing westerly winds. In this study, the inflow and surface forcing conditions are based on a realization of a weather model using realistic forcing and stratification. Studying wake dynamics under these realistic conditions enables us to analyze the wake behavior downstream of the farms as they might occur in the South Fork project. The objectives of this study are twofold: first, to capture the vorticity dynamics and analyze the competition between strain and vorticity in both the near and far wake regions, with a specific focus on how these dynamics influence the wake flow; second, to understand the turbulence induced by the wake and identify the dominant terms in the turbulent kinetic energy budget. This analysis captures the impact of the wake on the surrounding turbulent and overall circulation dynamics.

The present paper is structured as follows: section 2 describes the LES model and outputs. Section 3 presents the definition of wake regions, wake deficit decompositions, the wake vorticity budget, and turbulent kinetic energy budget. Section 4.1 analyzes and discusses the wake circulation dynamics. Section 4.2 describes and discusses the wake energy transfers. Section 5 provides conclusions.

2 LES Data Description

The LES model of Matheou & Chung [33] is used to model the turbulent flow of the MABL over the South Fork wind farm. The LES model was applied and validated in various atmospheric boundary layer

conditions [34, 35, 36, 37, 38]. The model numerically integrates the density-weighted filtered conservation equations of mass, momentum, total water mixing ratio and liquid water potential temperature. The anelastic approximation is used to account for the density variation with height. The conservation equations are discretized on an f-plane with the fully conservative fourth-order scheme of [39] and an exact Poisson solver using discrete Fourier transforms to satisfy mass conservation [40]. Time integration uses a third-order Runge-Kutta scheme. The subgrid-scale (SGS) scheme is a buoyancy-adjusted stretched-vortex model previously used for neutral and stratified atmospheric turbulence [41, 42, 43].

In this study, two distinct simulations were conducted to investigate the impact of wind farms on the atmospheric boundary layer. The first simulation is performed as a baseline to analyze the inherent turbulence dynamics of the ABL without the presence of the wind farm. The second simulation incorporates the wind farm using 12 actuator-disc models to represent the effects of the turbines in the LES. The actuator disc model uses a uniform thrust coefficient $C_T \sim 1.3$. The turbine diameter is 200 m and the hub height is 140 m. A smooth normalized indicator function to distribute the turbine thrust forces is used [32].

The spatial extent of the simulations is 12 km $\times$ 12 km $\times$ 1 km in the (x, y, z) dimensions, with a resolution of 10m across all dimensions. Periodic boundaries are used in the spanwise (y) direction, while inflow/outflow boundary conditions are applied in the streamwise direction (x). An auxiliary or precursor LES is used to generate the turbulent inflow condition. The inflow-outflow method described in [44] is used. The boundary conditions corresponding to the nighttime of June 16, 2020, are used. The local atmospheric conditions are taken from a simulation using Weather Research and Forecasting (WRF) model version 4.4 [45]. The WRF model configuration details are described in Zaman et al. [46]. WRF is a RANS model which results in mean atmospheric profiles of wind, temperature, humidity, and surface conditions. The precursor LES simulation is forced with the WRF-derived mean conditions such that fine-scale turbulence is generated consistent with the WRF-derived mean fields. A y-z vertical plane from the auxiliary LES is used as an inflow condition to the main LES simulation which includes the wind farm. The auxiliary and main LES are concurrent and synchronized [44]. The main LES is a free-running model without any artificial forcing or nudging, only in the precursor LES forcing is applied such that realistic turbulent inflow conditions are generated. Both LES simulations are spun up for one hour for the turbulence in the boundary layer to become established and reach a quasi steady state.

A Rayleigh damping layer is present at the LES domain top boundary to minimize gravity wave reflections. Surface fluxes are based on a uniform and constant sea surface temperature (SST) and are modeled using the Monin–Obukhov similariy theory [47]. For the present conditions, the SST is about 2 K warmer than the atmosphere. The surface conditions result in moderately convective conditions, with domain-averaged latent heat flux 345 $\mathrm{W\,m^{-2}}$ and sensible heat flux of about 133 $\mathrm{W\,m^{-2}}$.

The simulation outputs span 30 minutes with 60-second sampling. These outputs have been coarse-grained horizontally by 40×40 grid-point boxcar filter. Note that this filter has commutative properties with derivatives and integrals which is useful to our study.

Only the last 10 minutes of the wind farm simulation are used for the analysis. To match the simulated time between the two simulations given restart methods, the equivalent 10 minutes of the baseline simulation (shifted by 6 minutes in comparison to the wind farm simulation) were used as the period of analysis (Figure not shown). In this way, the two simulations are equivalent in time for turbulence to grow and be affected by surface fluxes, as well as the inertial oscillation phase and other aspects of the conditions.

3 Methodology

3.1 Definition of Wind Farms Regions

We have decomposed the actuator discs fields to address the definition of wind farms regions to wake deficit (wake deficit) and baseline (base) contributions. Each field can be written as a linear combination of these contributions:

$$\Xi = \Xi_{\text{base}} + \Xi_{\text{wake deficit}} \tag{1}$$

To separate the near wake and far wake downstream actuator discs, we used the minimum locations (x_0 and y_0) of the wake deficit variance [48]. The wake deficit variance is defined as:

$$\Delta\text{Var} = \text{Var}_{\text{wake deficit}} = \text{Var} - \text{Var}_{\text{base}} = 0.5 * (\text{u}'^2 - \text{u}'^2_{\text{base}} + \text{v}'^2 - \text{v}'^2_{\text{base}} + \text{w}'^2 - \text{w}'^2_{\text{base}}) \tag{2}$$

Perturbations used to generate the variance are defined as a deviation from a cross-flow y-average over the whole domain span (L_y):

$$\Xi' = \Xi - \frac{1}{\mathrm{L_y}} \int_0^{\mathrm{L_y}} \Xi \mathrm{dy} \tag{3}$$

Note that the variances themselves are not spatially averaged.

The near wake for each actuator disc is defined as $x - x_0 \in [-6D, 0]$ and $y - y_0 \in [-2D, 2D]$, while the far wake is defined as $x - x_0 \in [0, 15D]$ and $y - y_0 \in [-2D, 2D]$, where D ($\sim 200m$) is the diameter of the actuator disc (Figure 1).

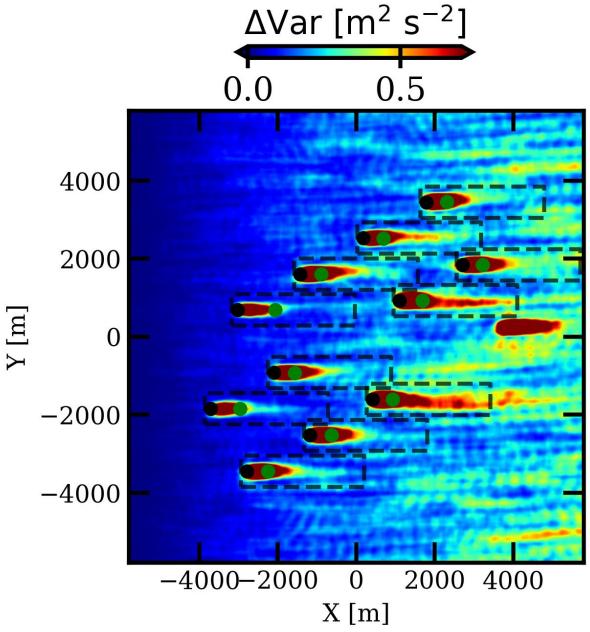

Figure 1: The time-averaged wake deficit variance (2) at the hub height. The black dashed boxes represent the downstream region of each actuator disc. The black dots indicates the location of the 11 actuator discs. The green dots indicates the location of the extremal wake deficit variance in each wake.

3.2 Wake Dynamics

For simplicity, the farm-scale variations in wakes will be neglected in this study. Thus, the wake dynamics will be assessed using the composite average, after aligning the location of the actuators, of the actuator discs' strain σ and vertical vorticity ζ_z in the different boxes illustrated in Figure 1, as defined below:

$$\zeta_z = \frac{1}{N} \sum_{i=1}^{N} (\partial_x v_i - \partial_y u_i) \tag{4}$$

$$\sigma = \frac{1}{N} \sum_{i=1}^{N} \left(\underbrace{(\partial_x u_i - \partial_y v_i)^2}_{\text{Tangential Strain}} + \underbrace{(\partial_x v_i + \partial_y u_i)^2}_{\text{Normal Strain}} \right)^{0.5} \tag{5}$$

where $N = 11$ is the total number of actuator discs used in the composite (see black dots in Figure 1).

We also aggregate the occurences of pointwise wake strain and vertical vorticity over the wakes of the 11 actuator discs analyzed. This aggregation provides statistics for the joint probability density function (jPDF) of strain and vorticity, as well as the conditional mean of divergence or other properties, as previously done in oceanic boundary layer studies of heterogeneous flows [49, 50]. To analyze these

statistics, We divided the jPDF and conditional mean into three distinct regions: anticyclonic vorticity-dominated (AVD) regions ($\zeta < 0$ and $\sigma < |\zeta|$), cyclonic vorticity dominated (CVD) regions ($\zeta > 0$ and $\sigma < |\zeta|$), and strain dominated (SD) regions ($\sigma \geq |\zeta|$).

Finally, we will link these dynamics to the composite- and time-averaged vertical vorticity budget for the composite disc wake to understand which terms are dominant in each region of the wake. The actuator discs vertical vorticity budget is given below:

$$\overline{\partial_t \zeta_z} + \underbrace{\overline{u_h \cdot \nabla_h \zeta_z}}_{h_{adv}} + \underbrace{\overline{w \partial_z \zeta_z}}_{v_{adv}} = \underbrace{\overline{(\zeta_z + f)\partial_z w}}_{\text{Stretching}} + \underbrace{\overline{\omega_h \cdot \nabla_h w}}_{\text{Tilting}} + \underbrace{\overline{\frac{1}{\rho^2}(\nabla \rho \times \nabla p) \cdot k}}_{\text{Baroclinic Torque}} + \text{Residuals} \tag{6}$$

where the terms on the right hand side from left to right are: the vorticity stretching (Stretching), the vorticity tilting (Tilting), the baroclinic torque and Residuals (mainly viscous torque and drag forcings curls caused by the actuator discs).

3.3 Wake Turbulence

Here we will define the actuator discs turbulent kinetic energy (TKE) budget analyzed in section 4.2. Here we define the TKE as the average of the deviations from the cross-stream average (i.e., the cross-stream averaged in the boxes displayed in figure 1)

The TKE budget is given below:

$$\overbrace{\partial_t k + \underbrace{\overline{u_j}\frac{\partial k}{\partial x_j}}_{\text{TKE advection}}}^{\frac{Dk}{Dt}} = -\overbrace{\underbrace{\frac{\partial}{\partial x_j}\overline{u_j' u_i' u_i'}}_{\text{Tr}^t} - \underbrace{\frac{1}{\rho_0}\frac{\partial}{\partial x_j}\left(\overline{u_j' p'}\right)}_{\text{Tr}^p}}^{\text{TKE Transport}} - \underbrace{\overline{u_i' u_j'}\frac{\partial \overline{u_i}}{\partial x_j}}_{\text{Shear Production}} + \underbrace{\overline{w' b'}}_{\text{Buoyancy Production}} + \text{Residuals} \tag{7}$$

where $k = \frac{1}{2}(\overline{u_i' u_i'})$, ρ_0 is the mean air density, TKE Advection is the advection of the actuator discs turbulent kinetic energy by the mean flow, Shear Production is a source of TKE (conversion from mean to turbulent kinetic energy), Buoyancy Production is the vertical buoyancy flux (conversion from turbulent potential energy to turbulent kinetic energy), Tr^p and Tr^t are the Transport of TKE by pressure and turbulence (Turbulent kinetic energy divergence and/or convergence), and residuals which are mainly Subgrid-Scale terms and turbines contributions. These budgets have been evaluated in each region of the farm and time averaged over the period of analysis.

4 Results

4.1 Wake Circulation dynamics

In this section, we will describe the actuator discs' downstream dynamics at the hub height, focusing on the characteristics of flow set out by the strain and vorticity pattern of the wake (Figure 2). Then, we will analyze the composite average of the actuator discs' composite wake vorticity budget.

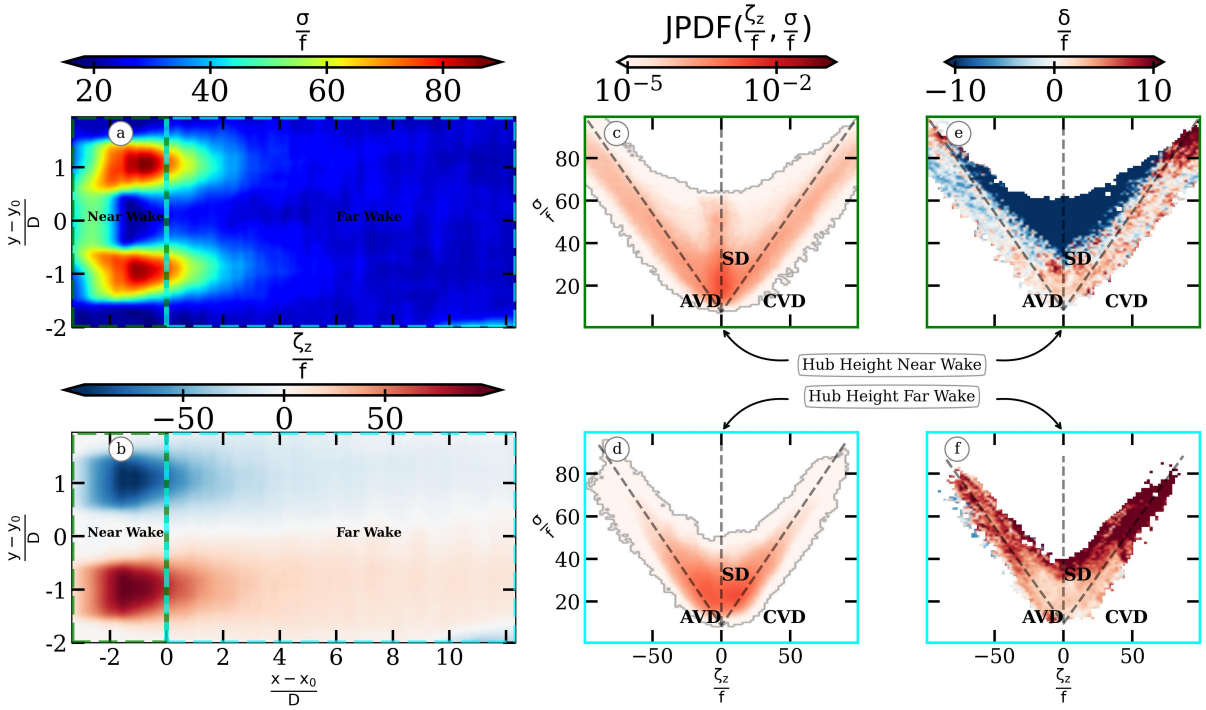

Figure 2: (a) and (b): Composite- and time-averaged strain and vertical vorticity at hub height, with green and cyan dashed boxes representing the near and far wake regions of the composite wake, respectively. (c) and (d): Aggregate jPDF of strain (vertical axis) and vertical vorticity (horizontal axis) normalized by the Coriolis parameter for near and far wake at hub height. (e) and (f): Conditional mean of horizontal divergence for near and far wake as a function of strain and vorticity at hub height.

At the hub height, the vertical vorticity and strain fields exhibit a nearly symmetric distribution downstream the actuator discs (Figure 2). In the near wake, straining motions and vortical structure coexist (Figure 2a and 2b). Their coexistence highlights distinct cyclonic and anticyclonic vortices separated by the wake axis ($\zeta_z \sim 0$). These cyclonic and anticyclonic features have relatively similar signatures in the strain vorticity fields ($\frac{\zeta_z}{f} \sim \pm 98$). In the far wake, the quasi-symmetric signatures of strain and vorticity decrease sharply, reflecting a transition to vortices breakdown and a more stable flow configuration induced by far-wake flow recovery [51].

These symmetric signatures in both regions are also revealed by the joint distribution of strain and vorticity highlighting a Gaussian-like structure in cross-section with fixed vorticity or strain (Figure 2c and 2d). This pattern is in good agreement with previous studies revealing the Gaussian distribution of the wake flow circulation [52]. In this distribution, the majority of the contribution (i.e., the most probable conditions) comes from the coexisting strain and cyclonic/anticyclonic regimes (JPDF > 0.2). In these regimes, the horizontal divergence is negative (convergent, more upward vertical velocity aloft) in the near wake (Figure 2e) and positive (divergent, more downward vertical velocity aloft) in the far wake (Figure 2f). The near-wake horizontal convergence favors vertical vortex stretching ($\partial_z w > 0$), for enhancement of ambient vorticity and therefore a circulation/enstrophy intensification (Figure not shown). In contrast, divergent flows in the far wake indicate vortex squashing ($\partial_z w < 0$) and thus tend toward a slower rotation rate and therefore a weakening in the circulation/enstrophy (Figure not shown). The far-wake divergence is part of the wake recovery mechanism which has been related in previous studies to lateral and vertical Reynolds shear stress gradients [53].

These dynamics are closely related to the vortex stretching and tilting, which are the main sources and sinks of circulation intensification or weakening. In the near wake, the cyclonic region (coexistence of strain and vorticity region) is subject to positive stretching and negative tilting; in contrast, the anticyclonic region is subject to negative stretching and positive tilting (Figure 3a and b). This indicates that both cyclonic and anticyclonic vortices are stretched, intensifying their circulation. This circulation intensification is accompanied by tilting converting streamwise vorticity into vertical vorticity with upward

motions along the wake axis. However, in the far wake, both vortices experience squashing which slows their circulation (Figure 3c). In the far wake, both stretching and tilting contributions decrease vertical vorticity (Figure 3d). The volume-averaged budget reveals a slower rotation rate downstream of the actuator discs ($\frac{D\zeta_z}{Dt} < 0$) as the signs of vorticity tilting and stretching oppose the flow vorticity in both anticyclonic and cyclonic regions (Figure 3e). This analysis connects the convergence, stretching, and tilting patterns in explaining the far-wake flow recovery due to a slowing down circulation. Previous studies [54] have shown similar dynamics related to tip vortices.

In summary, downstream of the farms, vortex stretching intensifies vorticity in the near wake, intensifying the circulation while tilting produces streamwise vorticity with upward motions along the wake axis. Meanwhile, both stretching and tilting reduce ambient vertical vorticity in the far wake and weaken the circulation as part of the flow recovery mechanisms.

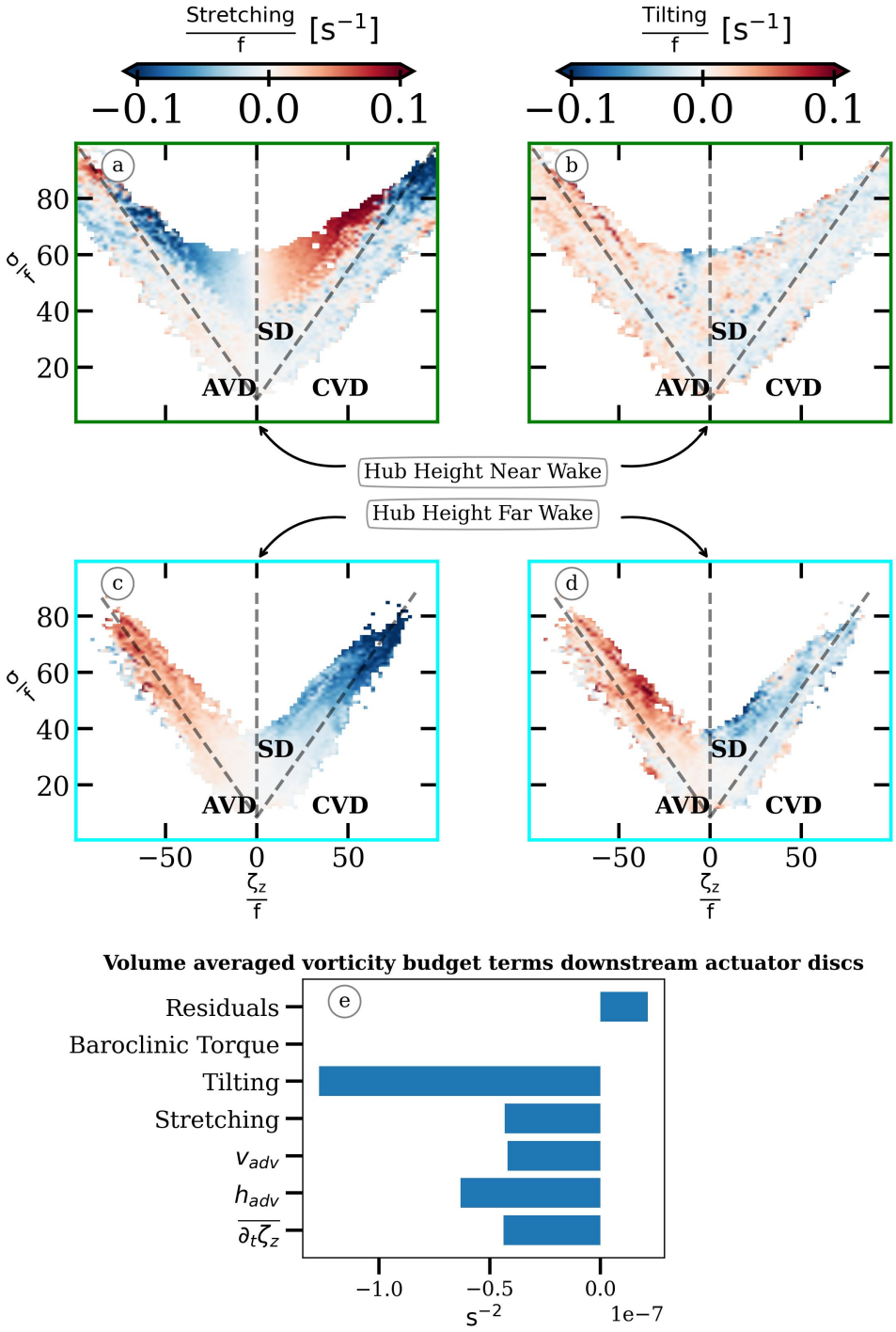

Figure 3: (a) and (b): Near Wake conditional mean of stretching and tilting in the near wake. (c) and (d): Far Wake conditional mean of stretching and tilting in the far wake. (e): Volume-averaged vorticity budget (includes both cyclonic and anticyclonic regimes) terms downstream of the actuator discs.

4.2 Wake Energy Transfers

In this section, we describe the turbulence production downstream of the actuator discs, diagnosing the wake deficit mean flow in both the near and far wake, and linking this deficit to the turbulent kinetic energy (TKE) budget.

Downstream of the actuator discs, most of the kinetic energy is extracted in the streamwise direction, as illustrated in Figure 4. The streamwise velocity deficit increases below the hub height, peaks around it, and subsequently decreases above, indicating a pronounced impact on the inflow dynamics (Figure 4a). Additionally, the actuator discs influence vertical motions; specifically, the positive wake deficit vertical velocity increases below the hub height and diminishes significantly at heights greater than 200 m, highlighting intense vertical motions within the wake (Figure 4c). This wake deficit also affects stratification, with temperature and humidity showing weak to moderate changes, particularly above the hub height, where the local environment becomes more humid (Figure 4e), consistent with the horzontal convergence and vertical stretching noted to be important for vorticity above. Notably, while these effects diminish in the far wake—especially concerning wind velocity—the wake deficit continues to play a crucial role in stratification, even above the hub height. This effect aligns with findings in the literature of observed wake patterns, where similar patterns of kinetic energy extraction and stratification changes have been documented [55, 56]. These variations in kinetic energy and stratification are linked to energy dissipation and turbulent production in the wake region.

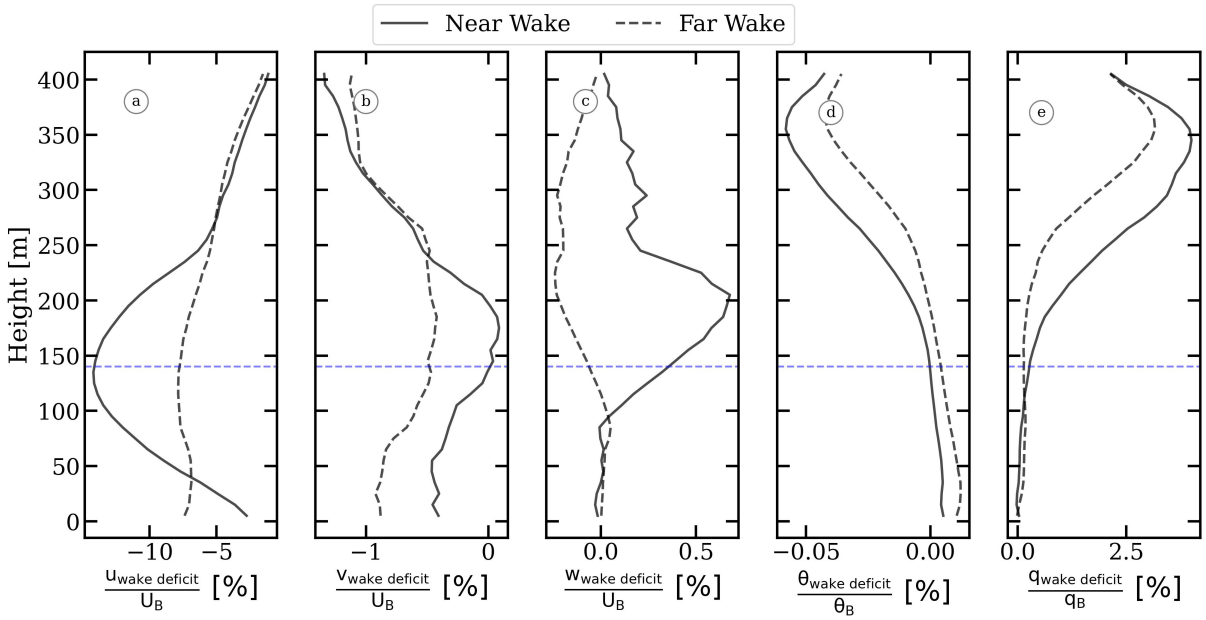

Figure 4: Wake deficit streamwise (a), spanwise (b), and vertical (c) velocities normalized by base flow magnitude. (e) and (f): Potential temperature and humidity normalized by base flow values. The black dashed line indicates hub height.

The variations in wake deficit velocity are associated with turbulent kinetic energy (TKE), which exceeds the base flow TKE, as shown in Figure 5a and Figure 1. The TKE is particularly intense in the near wake, between the bottom tip and top tip of the actuator discs. The primary source of this intensification is the production term of turbulent kinetic energy ($\frac{Dk}{Dt}$), as illustrated in Figures 5b and 5c. This term reaches its maximum above the hub height, where most of the conversion from mean kinetic energy to turbulent kinetic energy occurs near the top tip. In contrast, in the far wake, shear production acts as a sink for turbulent kinetic energy, suggesting that background mixing becomes crucial for facilitating flow recovery. Overall, the production of TKE in the near wake exceeds its sink in the far wake, as shown in Figure 5d. Downstream of the actuator discs, the transport term acts to remove TKE, while production serves as the main source, with buoyancy flux remaining positive—typical of nocturnal summertime boundary layers. These results align well with [57], where it is shown that shear production

and dissipation peak around the top tip, while the transport term removes TKE from regions above the wind farm and redistributes it below.

In summary, the main source of turbulent kinetic energy downstream of the actuator discs is shear production, peaking above the hub height, particularly at the top tip. The consistently positive buoyancy flux corroborates the dynamics of nocturnal boundary layers. Overall, TKE is generally removed through dissipation and transport.

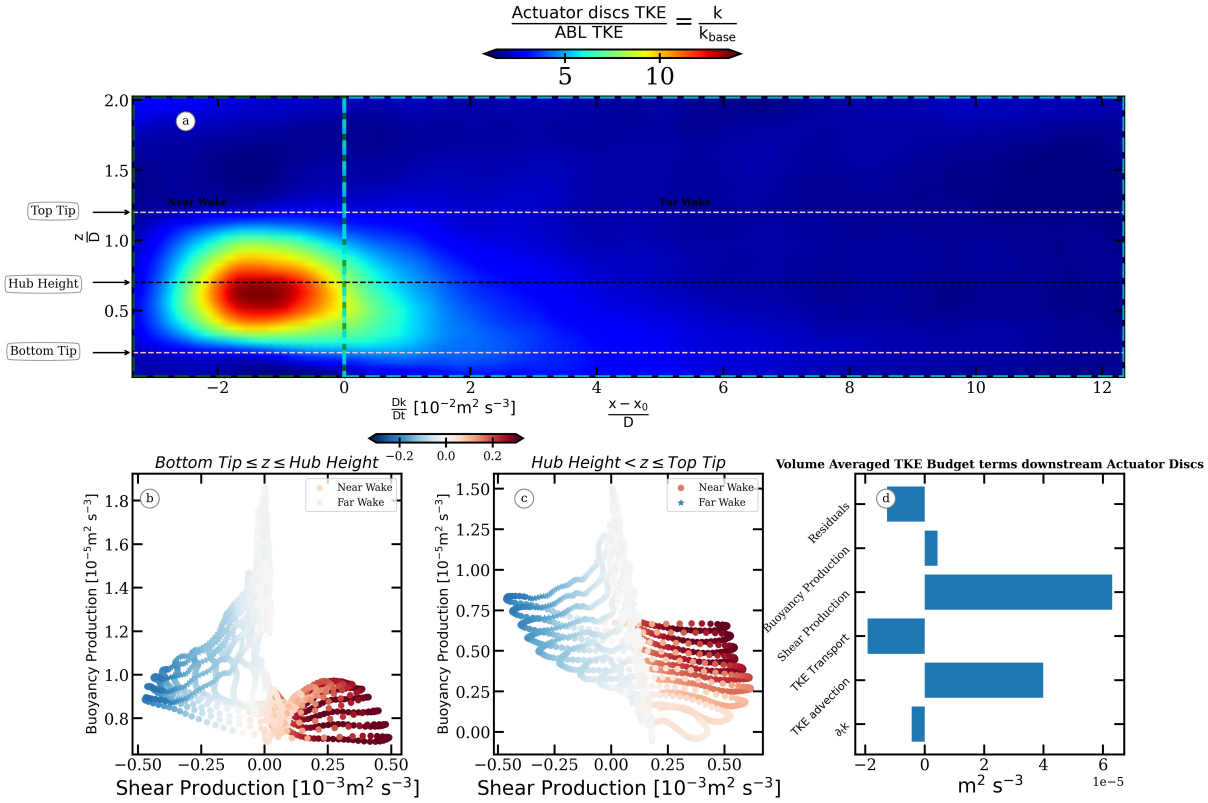

Figure 5: (a): Composite time-averaged actuator disc TKE normalized by base flow TKE, with green and cyan dashed boxes for near and far wake regions, and horizontal black and pink lines for hub height and actuator disc tips. (b): Scatter Plot of the material derivative of TKE as a function of shear production and Buoyancy production from the bottom tip to the hub height. (c): same as (b) from the hub height to the top tip. (d): Volume-averaged TKE budget terms downstream of the actuator discs.

5 Conclusions

We have investigated turbulence and circulation dynamics in the wake regions of the South Fork wind farms under realistic nocturnal forcing conditions. The main findings are that, downstream of the farms, tilting and stretching serve as sources of vorticity in the near wake, intensifying circulation and leading to convergent (upward) motions. Conversely, stretching and tilting act as sinks of vorticity in the far wake, weakening circulation and potentially facilitating flow recovery mechanisms. Additionally, shear production is the primary source of turbulent kinetic energy (TKE) downstream of the actuator discs, which peaks above the hub height, particularly at the top tip. The consistently positive buoyancy flux corroborates the dynamics of nocturnal summertime boundary layers, including a (small) positive buoyancy production indicating convection, while TKE is generally removed through dissipation and transport.

Future work will investigate the variability of these dynamics across convective, neutral, and stable boundary layers, considering the strength of stratification and variable inflow directions and magnitudes. We will also adopt an alternative perspective to mean TKE and vorticity budgets by employing structure functions [58] budgets that are not as reliant on filtering, as done in this study. This approach will

reveal turbulent length scales and the interactions between the wake, wake-to-wake dynamics, and the surrounding environment while being less sensitive to (arbitrary) choices of filter.

Acknowledgments
This work was supported by US Department of Energy grant DE-SC0024572. We acknowledge the support of Eversource Energy Center at the University of Connecticut. The research presented in this paper was supported by the systems, services and capabilities provided by the University of Connecticut High Performance Computing (HPC) facility.

References

[1] US Department of Energy 2008 20% Wind Energy by 2030 Increasing Wind Energy's Contribution to U.S. Electricity Supply https://www1.eere.energy.gov/wind/pdfs/42864.pdf

[2] Hansen M O 2017 Chapter 9 - aerodynamics and design of horizontal-axis wind turbines *Wind Energy Engineering* ed Letcher T M (Academic Press) pp 161–184 ISBN 978-0-12-809451-8 URL https://www.sciencedirect.com/science/article/pii/B9780128094518000096

[3] Porté-Agel F, Bastankhah M and Shamsoddin S 2020 *Boundary-Layer Meteorology* **174** 1–59 (*Preprint* https://doi.org/10.1007/s10546-019-00473-0)

[4] Schultze L K P, Merckelbach L M, Horstmann J, Raasch S and Carpenter J R 2020 *Journal of Geophysical Research: Oceans* **125** e2019JC015858 e2019JC015858 10.1029/2019JC015858 (*Preprint* https://agupubs.onlinelibrary.wiley.com/doi/pdf/10.1029/2019JC015858) URL https://agupubs.onlinelibrary.wiley.com/doi/abs/10.1029/2019JC015858

[5] Klemmer K S and Howland M F 2024 *Phys. Rev. Fluids* **9**(11) 114607 URL https://link.aps.org/doi/10.1103/PhysRevFluids.9.114607

[6] Rajewski D, Takle E, VanLoocke A and Purdy S 2020 *Geophysical Research Letters* **47** e2019GL086010 e2019GL086010 2019GL086010 (*Preprint* https://agupubs.onlinelibrary.wiley.com/doi/pdf/10.1029/2019GL086010) URL https://agupubs.onlinelibrary.wiley.com/doi/abs/10.1029/2019GL086010

[7] Liu Z, Li W, Shen L, Han Y, Zhu Z and Hua X 2021 *Building and Environment* **193** 107625 ISSN 0360-1323 URL https://www.sciencedirect.com/science/article/pii/S0360132321000378

[8] Baidya Roy S, Pacala S W and Walko R L 2004 *Journal of Geophysical Research: Atmospheres* **109** (*Preprint* https://agupubs.onlinelibrary.wiley.com/doi/pdf/10.1029/2004JD004763) URL https://agupubs.onlinelibrary.wiley.com/doi/abs/10.1029/2004JD004763

[9] Wang Q, Luo K, Wu C and Fan J 2019 *Energy* **183** 1136–1149 ISSN 0360-5442 URL https://www.sciencedirect.com/science/article/pii/S0360544219313532

[10] Kaytancı T, Menteş S and Ünal Y 2022 *Atmosphere* **13** ISSN 2073-4433 URL https://www.mdpi.com/2073-4433/13/11/1838

[11] Bhaganagar K and Debnath M 2014 *Energies* **7** 5740–5763 ISSN 1996-1073 URL https://www.mdpi.com/1996-1073/7/9/5740

[12] Bhaganagar K and Debnath M 2015 *Journal of Renewable and Sustainable Energy* **7** 013124 ISSN 1941-7012 (*Preprint* https://pubs.aip.org/aip/jrse/article-pdf/doi/10.1063/1.4907687/15867415/013124_1_online.pdf) URL https://doi.org/10.1063/1.4907687

[13] Khan M A, Javed A, Shakir S and Syed A H 2021 *Applied Energy* **298** 117229 ISSN 0306-2619 URL https://www.sciencedirect.com/science/article/pii/S0306261921006516

[14] Mahdi Abkar A S and Porté-Agel F 2016 *Journal of Turbulence* **17** 420–441 (*Preprint* https://doi.org/10.1080/14685248.2015.1127379) URL https://doi.org/10.1080/14685248.2015.1127379

[15] Dörenkämper M, Witha B, Steinfeld G, Heinemann D and Kühn M 2015 *Journal of Wind Engineering and Industrial Aerodynamics* **144** 146–153 ISSN 0167-6105 selected papers from the 6th International Symposium on Computational Wind Engineering CWE 2014 URL https://www.sciencedirect.com/science/article/pii/S0167610514002694

[16] Heck K S and Howland M F 2024 Coriolis effects on wind turbine wakes across atmospheric boundary layer regimes (*Preprint* 2403.12190) URL https://arxiv.org/abs/2403.12190

[17] Cheung L, Yalla G, Brown K, deVelder N, Hsieh A, Herges T, Houck D, Maniaci D, Sakievich P and Abraham A 2024 *Journal of Renewable and Sustainable Energy* **16** 063304 ISSN 1941-7012 (*Preprint* https://pubs.aip.org/aip/jrse/article-pdf/doi/10.1063/5.0211722/20249955/063304_1_5.0211722.pdf) URL https://doi.org/10.1063/5.0211722

[18] N Meroney R, Leitl B M, Rafailidis S and Schatzmann M 1999 *Journal of Wind Engineering and Industrial Aerodynamics* **81** 333–345 ISSN 0167-6105 URL https://www.sciencedirect.com/science/article/pii/S0167610599000288

[19] Tian L, Zhao N, Wang T, Zhu W and Shen W 2018 *Journal of Wind Engineering and Industrial Aerodynamics* **179** 215–228 ISSN 0167-6105 URL https://www.sciencedirect.com/science/article/pii/S0167610517306979

[20] Jia H, Lin C, Wang X and Kikumoto H 2024 *Boundary-Layer Meteorology* **190** 45

[21] Ayouche A, Fox-Kemper B and Laxague N J M 2025 (20pp, in preparation) *Renewable Energy*

[22] Shaw W, Berg L, Debnath M, Deskos G, Draxl C, Ghate V, Hasager C, Kotamarthi R, Mirocha J, Muradyan P *et al.* 2022 *Wind Energy Science* **7** 2307–2334 URL https://doi.org/10.5194/wes-7-2307-2022

[23] Bastankhah M and Porté-Agel F 2014 *Renewable Energy* **70** 116–123 ISSN 0960-1481 special issue on aerodynamics of offshore wind energy systems and wakes URL https://www.sciencedirect.com/science/article/pii/S0960148114000317

[24] Niayifar A and Porté-Agel F 2016 *Energies* **9** ISSN 1996-1073 URL https://www.mdpi.com/1996-1073/9/9/741

[25] Crespo A and Herna´ndez J 1996 *Journal of Wind Engineering and Industrial Aerodynamics* **61** 71–85 ISSN 0167-6105 URL https://www.sciencedirect.com/science/article/pii/016761059500033X

[26] Martínez-Tossas L A, Annoni J, Fleming P A and Churchfield M J 2019 *Wind Energy Science* **4** 127–138 URL https://wes.copernicus.org/articles/4/127/2019/

[27] Martínez-Tossas L A, King J, Quon E, Bay C J, Mudafort R, Hamilton N, Howland M F and Fleming P A 2021 *Wind Energy Science* **6** 555–570 URL https://wes.copernicus.org/articles/6/555/2021/

[28] Keck R E, Veldkamp D, Madsen H A and Larsen G 2012 *Journal of Solar Energy Engineering* **134** 021012 ISSN 0199-6231 (*Preprint* https://asmedigitalcollection.asme.org/solarenergyengineering/article-pdf/134/2/021012/5696721/021012_1.pdf) URL https://doi.org/10.1115/1.4006038

[29] Keck R E, de Maré M, Churchfield M J, Lee S, Larsen G and Aagaard Madsen H 2014 *Wind Energy* **17** 1689–1710 (*Preprint* https://onlinelibrary.wiley.com/doi/pdf/10.1002/we.1662) URL https://onlinelibrary.wiley.com/doi/abs/10.1002/we.1662

[30] Baungaard M, van der Laan M P and Kelly M 2022 *Wind Energy Science* **7** 783–800 URL https://wes.copernicus.org/articles/7/783/2022/

[31] Wang Q, Ti Z, Yang S, Yang K, Wang J and Deng X 2025 *Applied Energy* **378** 124812 ISSN 0306-2619 URL https://www.sciencedirect.com/science/article/pii/S0306261924021950

[32] Stevens R J, Martínez-Tossas L A and Meneveau C 2018 *Renewable Energy* **116** 470–478 ISSN 0960-1481 URL https://www.sciencedirect.com/science/article/pii/S0960148117308339

[33] Matheou G and Chung D 2014 *Journal of the Atmospheric Sciences* **71** 4439 – 4460 URL https://journals.ametsoc.org/view/journals/atsc/71/12/jas-d-13-0306.1.xml

[34] Chung D, Matheou G and Teixeira J 2012 **69** 3264–3276

[35] Matheou G 2016 **142** 3050–3062

[36] Matheou G 2018 *Atmosphere* **9** 392

[37] Matheou G and Teixeira J 2019 **147** 2621–2639

[38] Lamaakel O and Matheou G 2021 *Journal of Computational Physics* **427** 110012 ISSN 0021-9991 URL https://www.sciencedirect.com/science/article/pii/S0021999120307865

[39] Morinishi Y, Lund T, Vasilyev O and Moin P 1998 *Journal of Computational Physics* **143** 90–124 ISSN 0021-9991 URL https://www.sciencedirect.com/science/article/pii/S0021999198959629

[40] Schumann U 1985 *Algorithms for direct numerical simulation of shear-periodic turbulence* (Berlin, Heidelberg: Springer Berlin Heidelberg) pp 492–496 ISBN 978-3-540-39144-9 URL https://doi.org/10.1007/3-540-13917-6_187

[41] Misra A and Pullin D I 1997 *Physics of Fluids* **9** 2443–2454 ISSN 1070-6631 (*Preprint* https://pubs.aip.org/aip/pof/article-pdf/9/8/2443/19261830/2443_1_online.pdf) URL https://doi.org/10.1063/1.869361

[42] Pullin D I 2000 *Physics of Fluids* **12** 2311–2319 ISSN 1070-6631 (*Preprint* https://pubs.aip.org/aip/pof/article-pdf/12/9/2311/19328012/2311_1_online.pdf) URL https://doi.org/10.1063/1.1287512

[43] Chung D and Matheou G 2014 *Journal of the Atmospheric Sciences* **71** 1863 – 1879 URL https://journals.ametsoc.org/view/journals/atsc/71/5/jas-d-13-0126.1.xml

[44] Inoue M, Matheou G and Teixeira J 2014 *Monthly Weather Review* **142** 3418 – 3424 URL https://journals.ametsoc.org/view/journals/mwre/142/9/mwr-d-13-00400.1.xml

[45] Skamarock W C, Klemp J B, Dudhia J, Gill D O, Barker D M, Duda M G, Huang X Y, Wang W, Powers J G *et al.* 2008 *NCAR technical note* **475** 10–5065

[46] Zaman T, Juliano T W, Hawbecker P and Astitha M 2024 *Energies* **17** ISSN 1996-1073 URL https://www.mdpi.com/1996-1073/17/11/2618

[47] Fox-Kemper B, Johnson L and Qiao F 2022 Ocean near-surface layers *Ocean Mixing* (Elsevier) pp 65–94 URL http://dx.doi.org/10.1016/B978-0-12-821512-8.00011-6

[48] Shariff K B and Guillou S S 2022 *Applied Ocean Research* **128** 103329 ISSN 0141-1187 URL https://www.sciencedirect.com/science/article/pii/S0141118722002619

[49] Shcherbina A Y, D'Asaro E A, Lee C M, Klymak J M, Molemaker M J and McWilliams J C 2013 *Geophysical Research Letters* **40** 4706–4711 (*Preprint* https://agupubs.onlinelibrary.wiley.com/doi/pdf/10.1002/grl.50919) URL https://agupubs.onlinelibrary.wiley.com/doi/abs/10.1002/grl.50919

[50] Balwada D, Xiao Q, Smith S, Abernathey R and Gray A R 2021 *Journal of Physical Oceanography* **51** 2883 – 2901 URL https://journals.ametsoc.org/view/journals/phoc/51/9/JPO-D-21-0016.1.xml

[51] Hodgkin A, Deskos G and Laizet S 2023 *International Journal of Heat and Fluid Flow* **102** 109165 ISSN 0142-727X URL https://www.sciencedirect.com/science/article/pii/S0142727X23000644

[52] Baruah A and Ponta F 2024 *Dynamics* **4** 97–118 ISSN 2673-8716 URL https://www.mdpi.com/2673-8716/4/1/6

[53] van der Laan M P, Baungaard M and Kelly M 2023 *Wind Energy Science* **8** 247–254 URL https://wes.copernicus.org/articles/8/247/2023/

[54] Cheng B, Sane S, Barbera G, Troolin D, Strand T and Deng X 2013 *Experiments in Fluids* **54**

[55] Pol S, Wenner A and Castillo L 2017 *Renewable Energy* **114** 1224–1231 ISSN 0960-1481 URL https://www.sciencedirect.com/science/article/pii/S096014811730695X

[56] Neunaber I 2022 *Turbulence of Wakes* (Cham: Springer International Publishing) pp 881–911 ISBN 978-3-030-31307-4 URL https://doi.org/10.1007/978-3-030-31307-4_45

[57] Abkar M and Porté-Agel F 2014 *Renewable Energy* **70** 142–152 ISSN 0960-1481 special issue on aerodynamics of offshore wind energy systems and wakes URL https://www.sciencedirect.com/science/article/pii/S0960148114002146

[58] Pearson B C, Pearson J L and Fox-Kemper B 2021 *Journal of Fluid Mechanics* **916** A49